International Journal of Biological Macromolecules 253 (2023) 126556

Contents lists available at ScienceDirect

International Journal of Biological Macromolecules

journal homepage: www.elsevier.com/locate/ijbiomac

Nanofibrillated cellulose originated from *Rhododendron ponticum* to produce scaffolds using 3D printing for biomedical applications

Tielidy A. de M. de Lima [a], Gabriel Goetten de Lima [a,b], Nimra Munir [c], Joana Raquel Teixeira Coutinho [d], Geoffrey Robert Mitchell [d], Washington L.E. Magalhães [e], Michael J.D. Nugent [a,*]

[a] *Materials Research Institute, Technological University of the Shannon: Midlands Midwest, N37HD68 Athlone, Ireland*
[b] *Programa de Pós-Graduação em Engenharia e Ciência dos Materiais—PIPE, Universidade Federal do Paraná, Curitiba 81531-980, Brazil*
[c] *Centre for Precision Engineering, Materials and Manufacturing (PEM Centre),Atlantic Technological University, ATU Sligo, Ash Lane, F91 YW50 Sligo, Ireland*
[d] *Centre for Rapid and Sustainable Product Development, Institute Polytechnic of Leiria, 2430-082 Marinha Grande, Portugal*
[e] *Embrapa Florestas, Colombo 83410-000, Brazil*

ARTICLE INFO

Keywords:
Invasive species
Plant-based materials
Ultra-fine friction grinder
Extrusion

ABSTRACT

Rhododendron ponticum is an invasive species that spreads rapidly and is described as one of the biggest threats to peatlands in Ireland. This study offers an innovative approach to utilizing Rhododendron waste. Initially, sawdust was submitted to a bleaching treatment and the nanofibrillated cellulose (NFC) was obtained using two different methods: ultra-fine friction grinding and twin-screw extrusion with the assistance of TEMPO (2,2,6,6-tetramethyl-1-piperidinyloxy) pre-treatment. The samples processed through twin-screw extrusion exhibited the presence of NFC at five intervals, as confirmed by TEM analysis. However, these samples displayed a higher diameter deviation compared to those processed through grinding alone. Notably, after 20 extrusion steps, the NFC diameter became more uniform, reaching approximately 35 nm. Sedimentation tests showed that extrusion produced more homogeneous cellulose size than the grinder method. However, FTIR characterization for the samples showed a unique band related to C-O-C glycosidic linkage. The results showed that grinding breaks these groups resulting in crystallinity values lower than extrusion, 50 % compared 60 %. Therefore, NFC with 20 steps by grinding was blended with polycaprolactone to produce a 3D scaffold using a 3D printer at different ratios of 1–5 % addition. The effect of 1 % of NFC was unique showing significant enhanced mechanical properties compared to pure polycaprolactone (PCL), additionally, the NFC does not exhibit toxicity so these materials show promise for biomedical applications.

1. Introduction

Invasive alien plants (IAPS) are considered one of the most important causes for biodiversity loss, along with habitat, climate change, pollution and overexploitation [1], besides being an ecological threat, it also has an impact economically and environmentally, by the spread of disease. Many species are introduced in a different flora for several reasons, but mostly due to human interference for ornamental plants, as is the case with Rhododendron in Ireland [2]. *Rhododendron ponticum* was introduced to Ireland during the 18th Century as an ornamental garden plant because of its attractive flower coloration that ranges from purple to pink [3]. However, this species presents many problems if it is not pruned entirely. Rhododendron grows vigorously when pruned, and any stump leftovers will grow back and, in most cases, will bloom in 3–4 years [4].

Among the reasons for working with an IAPS, includes the development of alternative products that can be commercially attractive for the encouragement of prune for aggregated value, which can be a potential alternative for Rhododendron species in which few works actually investigated the potential benefits for this plant. Birinci et al. [5] studied the addition of *Rhododendron luteum* and *Rhododendron ponticum* in pulp and paper production by Kraft-$NaBH_4$ method. The overall properties were found to be ideal for pulp and paper industry, presenting 77 % of holocellulose in *Rhododendron ponticum* [5]. Such high value presents a possibility to use this species for the production of microfibrillated cellulose by a mechanical process, an approach not yet

* Corresponding author.
E-mail addresses: a00278595@student.ait.ie (T.A.M. de Lima), washington.magalhaes@embrapa.br (W.L.E. Magalhães), mnugent@ait.ie (M.J.D. Nugent).

https://doi.org/10.1016/j.ijbiomac.2023.126556
Received 25 April 2023; Received in revised form 28 July 2023; Accepted 25 August 2023
Available online 26 August 2023

investigated.

This work aims to obtain nanofibrillated cellulose (NFC) from *Rhododendron ponticum* from bleached pulp and bleached pulp oxidized with TEMPO (2,2,6,6-tetramethylpiperidine-1-oxyl radical) by two mechanical defibrillation methodologies, extruder and ultra-fine friction grinder. The utilization of TEMPO (2,2,6,6-tetramethyl-1-piperidinyloxy) as a pre-treatment method offers several advantages compared to other chemical pre-treatment methods. TEMPO oxidation is widely recognized as one of the most promising, efficient, and energy-saving approaches for converting plant cellulose fibers into nanofibers. This process involves the oxidation of polysaccharides, leading to the introduction of sodium carboxyl groups on the surfaces of elementary cellulose fibrils [6]. By employing TEMPO as the pre-treatment method, we can achieve controlled oxidation of the cellulose fibers, resulting in the production of nanofibers with enhanced properties. The introduction of carboxyl groups on the fiber surfaces enhances their dispersibility and compatibility with other polymers, facilitating their incorporation into various composite materials [7]. Furthermore, TEMPO pre-treatment enables us to obtain NFC with a targeted size and morphology. In our study, the TEMPO-treated samples exhibited NFC with an average diameter of 35 nm, indicating successful fibrillation and size reduction [8].

The extraction of NFC can be performed by defibrillating with various mechanical methods such as twin screw extruder [7], microfluidization, grinding [8], electrospinning [9,10], high intensity ultrasonication [11] and cryocrushing [12]. Through the fibrillation process, cellulose fibers are separated into a three-dimensional network of nanofibrils, which significantly increases the surface area available for interaction.

In this study, twin-screw extrusion (TSE) and ultra-fine friction grinder were used for the defibrillation process. Twin-screw extrusion has been recognized as an important method for NFC extraction, although it may have limitations such as relatively low yield. On the other hand, the grinder offers a cost-effective and easily accessible method. The choice between these two methods is primarily based on availability, scalability, and ability to control the fibrillation rate by repeating the shear forces through multiple steps using the equipment. Twin-screw extrusion equipment is also commonly available in industry. By comparing the extraction results obtained from both methods, we aim to provide valuable insights into their respective performance and suitability for NFC production.

Previous literature already studied the effect of defibrillation using a twin-screw extruder (TSE) on the pulp fiber properties, in terms of the degree of fibrillation and degradation [13–15]. This extrusion defibrillation process has many advantages such as high-shear homogenization, the possibility to obtain NFC with a concentration of 25–40 wt% fiber suspension, in some cases 50 wt%, which is a remarkably high solid content [7,13].This high concentration of cellulose in the suspension is very important for industries, considering transportation, production and storage (storage volume and shelf life). Therefore, a cellulose pulp extrusion process would be very attractive due to low production costs, related to high efficiency and fast processing [7,13].

In order to compare the fibers produced, defibrillation was also performed using an ultra-fine friction grinder, a widely used procedure for the production of NFC [16–19]. In this method, pulp underwent through a pair of grinding stones, where one stone is fixed while the other stone rotates [20]. The pulp is converted to nanoscale through the shearing of these grinding mechanisms, breaking the hydrogen bond and cell wall structure of the fibers. This method is known for the reduction of crystallinity and producing uniform suspension in NFC [21,22]. Although it is possible to obtain NFC with a higher number of steps using the grinding approach with 5, 15, 30, 60 and 120 steps [8]. These approaches are only possible with a diluted system with 1 wt% of cellulose raw material in the solution. For a concentrated system, higher than 3 wt %, the maximum of grinding steps for NFC is 20 steps. In order to compare both mechanical processes, with the same number of steps 5, 10 and 20 steps were chosen.

NFC has emerged as a promising polymer reinforcement material, offering a range of benefits such as moderate degradability, excellent surface expansion, and significant enhancement of mechanical properties [23]. It can be easily incorporated into hydrophilic polymers, further expanding its potential applications. Building upon these advantages, this study focuses on the production of scaffolds using NFC and polycaprolactone (PCL) as the matrix material, employing a 3D printer for potential biomedical applications [24]. PCL was selected due to its compatibility with 3D printing techniques, while demonstrating excellent biocompatibility and reasonable mechanical properties [25–28]. By blending NFC with PCL, not only can the mechanical properties be improved, but also the biocompatibility can be maintained, opening up new possibilities for drug delivery devices and other biomedical applications.

2. Materials and methods

Polycaprolactone (PCL, Sigma-Aldrich, USA, Mw = (70,000–90,000 g/mol)) and 2,2,6,6-tetramethylpiperidine-1-oxyl radical (TEMPO) were purchased from Sigma-Aldrich (St. Louis, MO, USA), and used as received. *Rhododendron ponticum* branches were harvested from the Conemara National Park, city of Gayway, in Ireland. These samples were donated by ATU Galway Campus. Before starting the analysis, the samples were grounded in order to obtain the sawdust. Then, chemical pre-treatment was performed before defibrillation for obtain the bleached pulp.

2.1. Sawdust pre-treatment

2.1.1. Bleaching

The standard TAPPI T9 wd-75 [29] was used to perform the bleaching. In this treatment, lignin and extractives were removed, allowing only holocellulose in the structure. For this, 100 g of sawdust were added to 1000 mL of water containing 30 g of sodium chlorite and 5 mL of acetic acid; this solution was heated for 60 min at 70–80 °C. This step was repeated every 60 min until the total bleaching of the sample was verified, which occurred after six steps. This treatment was referred to samples as bleached.

2.1.2. Oxidation with TEMPO

After sawdust bleaching, part of the sawdust was used for an oxidation that was performed in the fibers using 2,2,6,6-tetramethylpiperidine-1-oxyl radical (TEMPO)-mediated oxidation under moderate aqueous conditions. 5 g of cellulose pulp was dispersed in a 0.05 M sodium phosphate buffer solution (500 mL, pH 7) containing 200 mg of TEMPO. 4 g of sodium chlorite and 20 mL of NaClO solution were added to the beaker and the fiber suspension was kept under magnetic stirring at 60 °C for 12 h. Then, the fibers were recovered by filtration, washed three times with deionized water and the consistency was adjusted to 10 % by vacuum filtration of the fiber suspension [7].

2.2. Production of the nanosuspension of Rhododendron

2.2.1. Defibrillation process with a twin-screw extruder (TSE)

Prior to extrusion, the solid content of the bleaching and TEMPO samples were adjusted to ca. 24 wt% by removing the excess water in the pulp as describe for Ho et al. [13]. The pulp was then fed into the TSE [twin screw extruder, baby prism]. The operating temperature of the TSE was set to 0 °C. This temperature was controlled to be as close to 0 °C as possible, and the kneading part of the extruder never exceeded 40 °C. The screw speed was 100 rpm [15]. The pulp material was kneaded 20 times through the TSE. Samples were taken at 5×, 10× and 20× steps to compare fiber size throughout the defibrillation process. To disperse this kneaded powder in water for further characterization, it was diluted into an aqueous cellulose suspension of ca. 1 wt% and

afterwards, homogenized with an ultra turrax for 5 min in 10 k rpm. As a result, the following samples were obtained: EB5x, EB 10x, EB20x and ET5x, ET10x and ET20x, where EB is related to extrusion with bleaching and ET related to extrusion with TEMPO.

2.2.2. Defibrillation process with a grinding

The samples grinded with bleach (GB) and grinded with TEMPO (GT) were prepared in a suspension with a concentration close to 31 %, using distillate water, then it was fragmented using a 450 W blender for 10 min. Subsequently, it was subjected to further grinding using a supermasscolloider, Masuko Sangyo Microfluidizer, using a rotation of 1500 rpm, 20 steps and distance between discs of 0.1 mm. Samples were taken at 5, 10 and 20 steps. As a result, the following samples were obtained: GB5x, GB 10x, GB20x and GT5x, GT10x and GT20x. In this process, the fibers are reduced to the nanometric size (0.1 and 100 nm) and through the friction between the stones, abrasive forces are introduced on the cellulose. With this procedure, it is possible to obtain a nanosuspension formulation that exhibits a gel-like characteristic [30].

Transmission electron microscopy was performed in all samples to observe the differences between each step through the mechanical defibrillation and the pre-treatments. However, for sedimentation speed analyses, XRD, FTIR and thermogravimetric analysis just the last step (EB20x, ET20x, GB20x and GT20x) was measured.

2.3. Chemical characterization

The content of ethanol-toluene extractives and Klason lignin were assessed following ASTM standards. The measurement of holocellulose content was conducted using the method described by literature [31]. All chemical quantifications were performed in triplicate.

2.4. Evaluation of the nanosuspension by transmission electron microscopy

The characteristic morphologies of the Rhododendron nanosuspension with bleaching and TEMPO were investigated using a transmission electron microscope (TEM) JEOL, model JEM-1200 EXII. For this, the NFC was diluted to 0.1 % w/v, dispersed in an ultrasonic bath for 20 min, and then cast on a copper TEM sample grid.

2.5. Sedimentation speed

50 mL of all aqueous cellulose suspensions with a solid content of 0.2 wt% was transferred to transparent bottles. This suspension was prepared using an ultra turrax for 5 min in 10 k rpm. The bottles were sealed being and left to stabilize. Pictures were taken immediately, then after 15 and 30 min, 1, 2, 8, 24, 48 h, 7 days and one month. The sedimentation of the suspensions was qualitatively evaluated based on the photographs [13].

2.6. X-ray diffraction spectroscopy (XRD)

Diffractograms were obtained using a Siemens D500 X-ray powder diffractometer (Karlsruhe, Germany) with Cu Kα radiation ($\lambda = 0.15418$ nm). The diffraction was examined in the range of 10° to 80°. The samples tested were the films produced through the solvent casting process. For this analysis, only step number 20 was tested after extrusion and grinder to observe differences in crystallinity in each mechanical and chemical process.

2.7. Fourier transform infrared spectroscopy (FTIR)

PerkinElmer Spectrum One Fourier transform infrared spectroscopy (FTIR) (PerkinElmer, Waltham, MA, USA) was used to investigate the difference between the micro-fibrillated cellulose produced by extrusion and grinder. The IR spectra were recorded in the spectral range of 1500–650 cm^{-1}, utilizing 4 scans per sample, and a fixed universal compression force of 80 N.

2.8. Thermogravimetric analysis

Films of cellulose were weighted around 4–5 mg and encapsulated in alumina sample pans for the thermogravimetric analysis (DTG). A temperature ramp for the TGA was set from 20 °C to 600 °C at a rate of 10 °C/min was used with an empty alumina pan as a reference. The experiments were carried out under nitrogen flow of 50 mL min^{-1}, in a Q600 SDT—TA Instruments (TA Instruments, New Castle, PA, USA).

2.9. Preparation of PCL/gel solution containing NFC

The mixture of PCL and NFC was performed by initially dissolving the PCL at a temperature of 90 °C. For the production of these scaffolds, the NFC produced by the grinding process and with TEMPO was chosen (GT20X). After dissolving PCL, mixtures were produced at concentrations of 1 %, 2 % and 5 % of NFC using GT20x.

2.10. Fabrication of nanocomposite scaffolds

Scaffolds were produced using a bioextruder (Bioextruder system, developed by the Centre for Rapid and Sustainable Product Development, Polytechnic Institute of Leiria) through a nozzle with a diameter of 0.8 mm. Scaffolds with dimensions of 16 × 16 × 4 mm and pore configuration of 0°/90°, were processed at 115 °C, using deposition velocity of 300 mm/min and the screw rotation velocity of 40 rpm. The scaffolds prepared were PCL, PCL + 1 % NFC, PCL + 2 % NFC, PCL + 5 % NFC.

2.11. Scanning electron microscope (SEM)

The scaffolds surface was observed using a Mira scanning electron microscope (TESCAN Performance in Nanospace, Tescan Orsay Holding, Brno, Czech Republic) with the back-scattered electron (BSE) mode. Prior to imaging, specimens were sputtered with gold in Baltec SCD 005 for 110 s at 0.1 mbar vacuum yielding a coating of ca. 110 nm. The images were recorded at an acceleration voltage of 20 kV and a magnification of 50×.

2.12. Compression resistance tests for scaffolds

The mechanical test of compression resistance was performed using the Instron 4505 machine, load 10 kN. The crosshead travel speed was 1 mm/min. The height of each cylinder was measured before being placed on a support, and the downward vertical force was carried by the cell until complete rupture as described by Lopes et al. [32]. The 3D scaffolds test (16 × 16 × 4 mm) was conducted according to ASTM STP 1173 standards [33].

2.13. In vitro cytotoxicity assay

MTT colorimetric assay was used to evaluate the cytotoxicity potential of the scaffolds. The samples were sterilized using ethanol 70 % for 30 s, phosphate buffered saline (PBS) for 30 s, followed by DEMEM media for 30 s prior to cytotoxic evaluation following the methodology of a previous report [12,19]. The 3T3 cells were incubated at 37 °C and in a 5 % CO_2 incubator. Cells were then exposed to different concentrations. For the preparation of samples, 25 mg of each scaffold sample was weighed and diluted in 1 mL of DEMEM. In this experiment, concentrations of 25 mg mL^{-1}, 5 mg mL^{-1}, 1 mg mL^{-1} and 0.5 mg mL^{-1}were tested. After treatments, cells were washed with PBS before the addition of 100 μL serum-free media containing yellow tetrazolium salt dye (1 mg mL^{-1}) and incubated for 3 h at 37 °C. Next, the supernatant was removed, the residual purple formazan product solubilized in

200 μL dimethyl sulfoxide (DMSO), and its absorbance measured at 570 nm (BioTek Synergy HT, Swindon, UK). The absorbance of the negative control was set as 100 % viability and the values of treated cells were calculated as percentage of control.

2.14. Statistical analysis

The data were tested for normality by the Shapiro–Wilk test. Analysis of variance was performed. For parametric data, post-hoc Tukey-HSD was performed using agricolae R package.

3. Results and discussion

3.1. Chemical characterization

In this work, holocellulose was extracted via two chemical routes. The first one was bleaching using $NaClO_4$ and acetic acid, and the second one was oxidation with TEMPO after bleaching. Furthermore, chemical characterization (extractives, lignin, and holocellulose) was performed for the samples before and after the chemical treatment (Table 1). The sample after bleaching still contains extractives (0.5 %) and lignin (6 %). Some extractives can act as inhibitors of nanocellulose formation, reducing its production or negatively influencing its final properties. Albornoz-Palma et al. [34] studied the effect of residual lignin on LCNF properties, and concluded that there is no consensus on the effect of residual lignin on mechanical fibrillation due to its dual-effect, residual lignin that can either act as an antioxidant, facilitating fibrillation, or act as a cementing agent, impeding fibrillation and, consequently, the production of LCNFs [34]. Herein, the presence of lignin in the sample after bleaching reduced the defibrillation, resulting in larger fibers, as observed in Fig. 1 (EB and GB samples). Balea et al. [35] studied how pretreatment and mechanical nanofibrillation energy affect the properties of nanofibers derived from Aspen cellulose. They found that the lignin particles reduce the defibrillation effect using high-pressure homogenization [35].

The oxidation with TEMPO removes almost all of the extractives and lignin from the Rhododendron, it was not possible to quantify using the methods employed. Several studies in the literature demonstrate the production of nanowhiskers (with a lower aspect ratio than CNFs) using TEMPO as an oxidizing agent through various mechanical processes. By oxidizing the cellulose with TEMPO, the defibrillation process is enhanced, leading to the production of finer nanowhiskers [36,37].

3.2. Morphology of the nanosuspensions

The suspensions underwent transmission electron microscopy (TEM) to observe the dimensions and structures of the nanofibrils obtained by the extrusion and grinder process. In addition to the mechanical process, the use of the oxidant TEMPO in the defibrillation of NFC was analyzed, in Fig. 1 it can be observed the micrographs of pulp suspensions for all treatments. Comparing the samples only with bleaching defibrillated by the extruder (EB) and the grinder (GB), the difference in the degree of defibrillation in each step can be observed, with the mechanical process being the only variable. After the extrusion process and varying the number of steps (Fig. 1a–c), micro-sized fibers are still visible. Using the grinder process (Fig. 1g–i) nanofibers can already be observed in the first passes. In the extruder process, the fiber size did not vary considerably as 5×, 10× and 20× cycles results in fibers of length, 90 nm, 100 nm and 96 nm, respectively (Fig. 1m–o). In grinding (Fig. 1s–u), these averages were 139 nm for 5×, 84 nm for 10× and 39 nm for 20×.

Many works in the literature uses TEMPO to oxidize the fibers before the mechanical process in order to improve the defibrillation [7,38–40]. When this treatment is carried out, NFC morphology can be observed in the extruder and the grinder process, see (Fig. 1d–f and j–l), respectively. Here, the averages for samples pre-treated with TEMPO can be observed. (Fig. 1p–r) and (Fig. 1v–z). Both in the extruder and in the grinding, the fiber sizes decrease in relation to the samples that were carried out only for bleaching.

Isogai et al. found significant amounts of clearly unfibrillated bundles and fibers still present in NFC after extrusion process, the fibers found were larger than 100 nm [40]. However, Trigui et al. observed that the successful defibrillation of fibers chemically treated by extrusion is favored by the swelling of the fibers, facilitating the breakdown of cell walls and the individualization of cellulose nanofibrils [7].

Bleached extruded fibers presented mean diameter values in the order of 96 nm after 20 steps. However, after TEMPO it reached 38 nm. When the grinding process was performed, bleached samples had diameters in the order of39 nm after 20 steps and TEMPO reached 35 nm after 20 steps. Therefore, at the last step, the process and methodology used to isolate the nanofibers did not interfere in the fiber size. However, bleached presented higher mean fiber diameter for extrusion process. Within the steps, extrusion presented already fibers in the range of nm already at 5 steps when TEMPO was performed, which remained relatively similar throughout the steps. However, grinding with TEMPO, although presenting smaller fibers diameters compared to bleach, only reached the sizes of ET at 20 steps.

The grinder process using TEMPO (GT) produces more defibrillated fibers than the extruder process. The grinder process is widely used in the literature for the production of NFC [41–44]. The difference in variation of fiber size between the extrusion and grinding processes can be attributed to the nature of shear forces and the concentration of cellulose during each method. In the extrusion process, the shear forces primarily occur between the fibers themselves due to the high concentration of cellulose (~25 %). As a result, there is relatively minimal contact between the fibers and the metal components of the extruder. This limited interaction between fibers and metal leads to a more uniform and consistent fiber size throughout the extrusion process. On the other hand, in the grinding process, the concentration of cellulose reaches a maximum of 3 %. As a result, the shear forces predominantly occur between the fibers and the grinding stone. This direct contact between the fibers and the stone facilitates more efficient defibrillation, resulting in a greater reduction in fiber size with each pass. Consequently, the grinding process exhibits a larger difference in fiber sizes between successive passes compared to extrusion.

Although TEMPO was effective in reducing the size of NFC during the grinding process, its efficacy was found to be comparatively lower than in extrusion. Further investigation is necessary to understand the specific mechanisms at play during extrusion and the shear forces involved in this technique. One potential reason for the observed difference could be attributed to the high viscosity encountered in the grinding process. As the stones rotate, shear forces are applied, but the defibrillation process is significantly hindered by the resistance of the nanosuspension against deformation, as dictated by its viscosity. With increased dispersity, there is a corresponding increase in viscosity, making it more challenging to achieve efficient defibrillation. On the other hand, extrusion offers advantages in terms of the volume and forces that can be exerted throughout the material. The shear strain rates in the final section of the extrusion process are relatively low, which allows for the successful extrusion of polymers with high molecular weights. This suggests that the extrusion process may facilitate the defibrillation process as well, potentially overcoming the viscosity-related challenges encountered in grinding. To gain a comprehensive understanding of the effects of extrusion, further tests and analyses are

Table 1
Chemical characterization (extractives, lignin and holocellulose) of *Rhododendron ponticum* before and after chemical treatment.

	Extractives (%)	Lignin (%)	Yield (%)
Rhododendron ponticum	2.64 ± 0.17	25.41 ± 0.12	–
Rhododendron after bleaching	0.5 ± 0.4	6.3 ± 0.3	75.4 ± 1.2
Rhododendron after TEMPO	–	–	44 ± 1.9

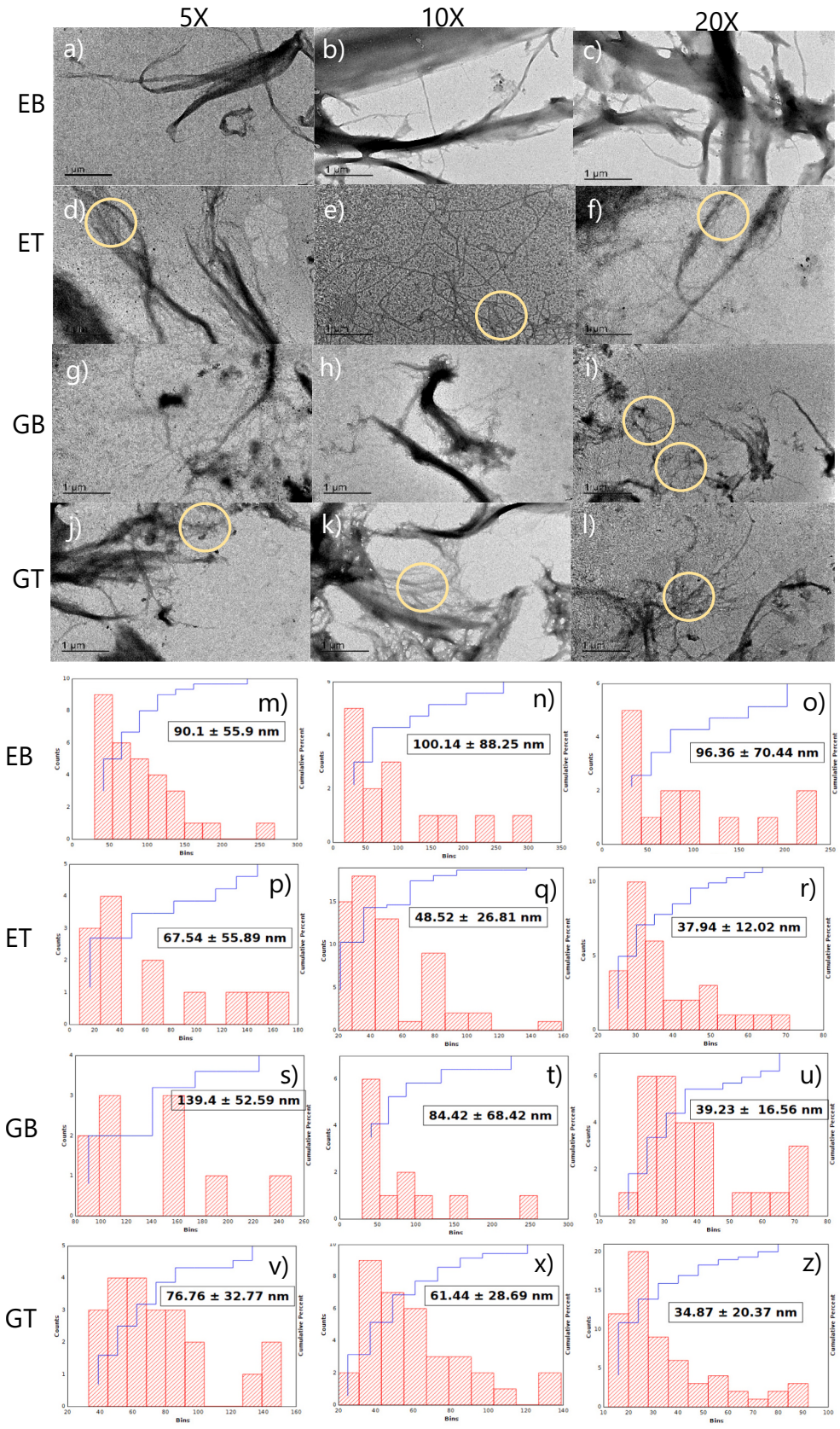

Fig. 1. Micrographs of the EB, ET, GB and GT suspensions with different steps: a) EB 5 steps, b) EB 10 steps, c) EB 20 steps, d) ET 5 steps, e) ET 10 steps, f) ET 20 steps g) GB 5 steps, h) GB 10 steps, i) GB 20 steps, j) GT 5 steps, k) GT 10 steps and l) GT 20 steps. All images are at 5000× magnification and with 1 µm scale. Measurements of fiber sizes in treatments m) EB 5 steps, n) EB 10 steps, o) EB 20 steps, p) ET 5 steps, q) ET 10 steps, r ET 20 steps s) GB 5 steps, t) GB 10 steps, u) GB 20 steps, v) GT 5 steps, x) GT 10 steps and z) GT 20 steps.

required. By investigating the specific conditions and shear forces present within the extrusion equipment, we can shed more light on the underlying mechanisms driving the defibrillation process. This knowledge will contribute to optimizing the production of NFC and enhancing its potential applications. Regarding internal defibrillation, it can be observed in Fig. 1 (yellow circles) where the process is occurring. Extrusion + bleaching exhibited no internal defibrillation in our samples. However, extrusion with tempo consistently exhibited internal defibrillation in all steps. For the grinding method, we observed different results. Initially, grinding with bleaching did not present internal defibrillation in the first steps, but it became apparent after 20 steps. On the other hand, grinding with Tempo consistently showed internal defibrillation in all steps.

3.3. Sedimentation speed

Photographs of cellulose fibers settlement after ten different time periods are shown in Fig. 2. The sedimentation of cellulose fibers was tested for all treatments (EB, ET, GB and GT) after 20 steps. The sample EB20 starts to sedimentation in the first 15 min of the analysis, and was sedimented after 1 h and remained relatively stable until the end of the analysis. As seen in the TEM the fibers, with 20 steps it is possible to see fibers not yet thoroughly defibrillated in the suspension. For the sample with TEMPO, ET20, the results were better. The sample started to sediment after 30 min but the speed of sedimentation decreases. For the grinder process, only after 24 h the first sedimentations appear. It is possible to see a thicker layer for the GB sample compared to the GT sample. The sample GT was the one that remained in suspension for the longest time in agreement with TEM. Ho et al. [13] studied the effect of the fibrillation process through a TSE on the properties of cellulose fibers. The authors noted that the higher the defibrillation steps, the longer the sample is suspended in water, the availability of hydroxy groups in native cellulosic structures is predominantly influenced by the size of the cellulose crystallite widths [45]. The sedimentation speed is a qualitative test to observe the stability of NFC in aqueous solutions. Many works in the literature use these NFC aqueous solutions for more diverse applications, one of the most well-known is Pickering emulsions, which is an emulsion stabilized by solid particles, and has several

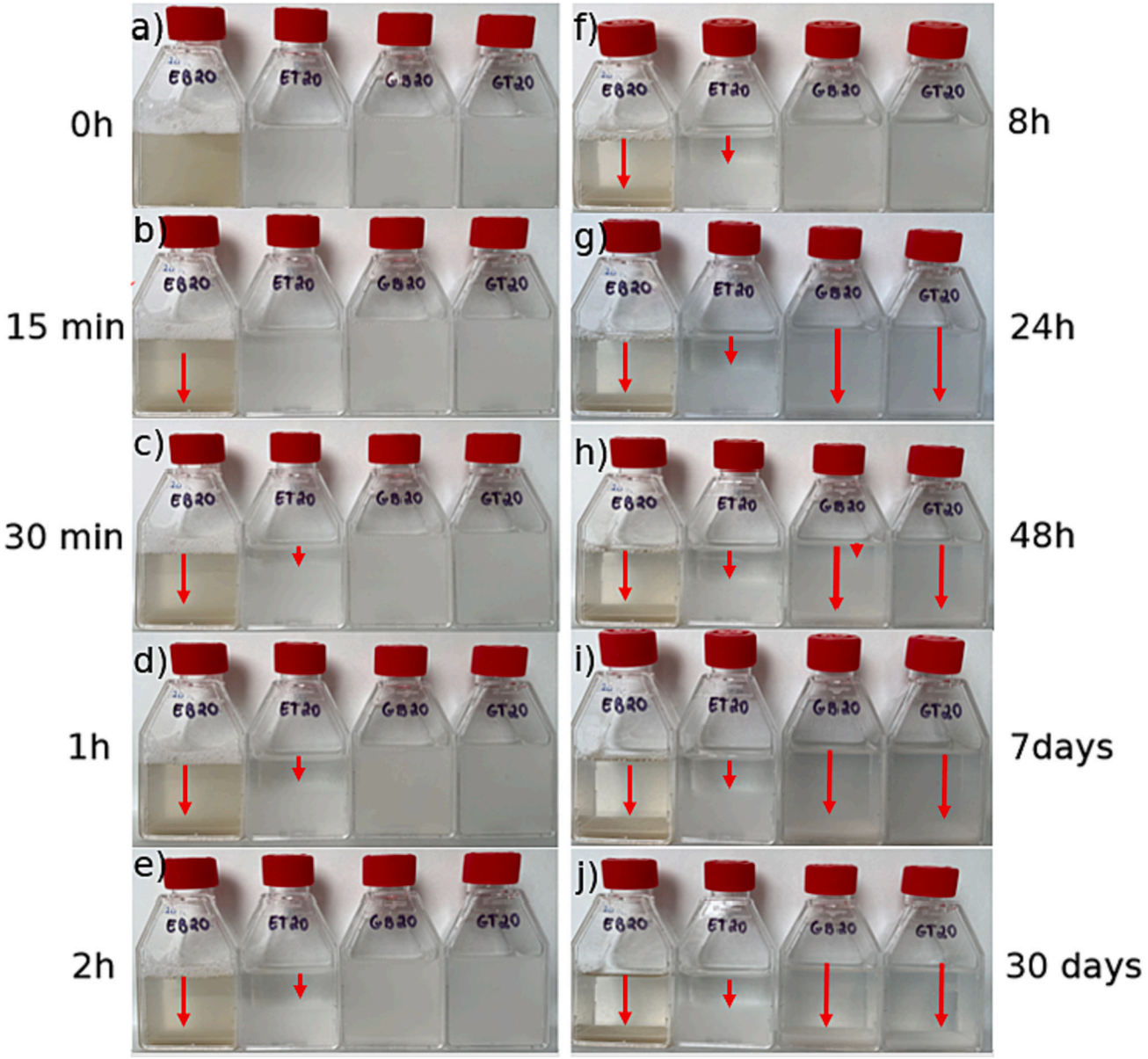

Fig. 2. Photographs after 0, 15 min, 30 min, 1 h, 2 h, 8 h, 24 h, 48 h, 7 days and 30 days, of aqueous suspensions of 0.2 wt% fibrillated cellulose with various passes through a TSE and grinder.

potential applications in the areas of drug delivery, food and composite materials [46].

3.4. Fourier transform infrared spectroscopy (FTIR)

The films obtained from the pulp suspensions by the extruder and from the pulp by the grinder were submitted to FTIR analysis. Fig. 3a shows the infrared spectrum of the films. The EB20x, ET20X, GB20X and GT20x film samples showed bands characteristic of cellulose, with similar absorbance bands with different intensities. Few new peaks were observed in the extruder or grinder process, which could mean that no new covalent bonds or functional groups had been formed [47]. The peaks in common for all samples were at the lengths of 3337 cm^{-1} (OH stretching intramolecular hydrogen bond), 2890 cm^{-1} (C—H symmetrical stretching), 1372 cm^{-1} (C—H bending in plane), 1155 cm^{-1} (C-OC glycoside ether band), 1048 cm^{-1} (C-O-C pyranose ring stretching vibration), 988 cm^{-1} (C—H aromatic hydrogen) 893 cm^{-1} (C-O-C, C-C-O, C-CH deformation and stretching, β-glycosidic) [48,49]. Hop et al. [50] studied the preparation of NCs from bleached wood pulps by TEMPO oxidation, there is a very tiny change in FTIR after oxidation. They found only a slight change in the peak at 1630, which shifted to 1600 cm^{-1} [50]. Overall samples presented similar profile whether the treatment or the process for nanofibrils isolation. However, for the extruder process only, a new peak appears in 1200 cm^{-1}, related to (O—H bending and C–O–C stretching of pyranose ring) [51]. Therefore, it is possible that the grinding mechanism reduces the chain length by breaking the C-O-C glycosidic linkage [52].

3.5. X-ray diffraction spectroscopy (XRD)

XRD was applied in this study to investigate the nature of the cellulose produced in each process. Based on the calculation method describe in literature [53], in which the percentage of crystalline cellulose is determined by the difference between the intensity of the crystalline peak (with greater intensity referring to plane 002) and the amorphous part, the average crystallinity index of samples EB20x, ET20x, GB20x and GT20x was determined (Fig. 3b). It can be seen that all cellulose samples showed 2 characteristic diffraction peaks at 2 theta angles of 16.0° and 22.8° corresponding to the (110) and (200) the most important planes of the cellulose crystal. The diffractogram profile was the same as found in the literature [54].

The measured crystallinity value for the sample EB20x, ET20x, GB20x and GT20x were 62.7 %, 60.4 %, 53.3 % and 50.21 % respectively, as it can be observed in Fig. 3b. Both the extrusion process and the process performed in the grinder decreased the crystallinity after chemical treatment with the TEMPO oxidant. The chemical treatment caused the degradation of the cellulose crystals regions, in agreement with the FTIR. In addition, it is found in the literature that the grinding process reduces the crystallinity of NFC [21,55].

The difference in CrI between the grinding and extrusion samples can be attributed to the distinct mechanical actions exerted during the two processes. In the case of grinding, the high shear forces applied by the equipment result in a significant disruption of the amorphous regions of the cellulose structure. Our previous studies have suggested that these shear forces, combined with the apparent density of the cellulose, contribute to a change in the packing molecular ordering, leading to a

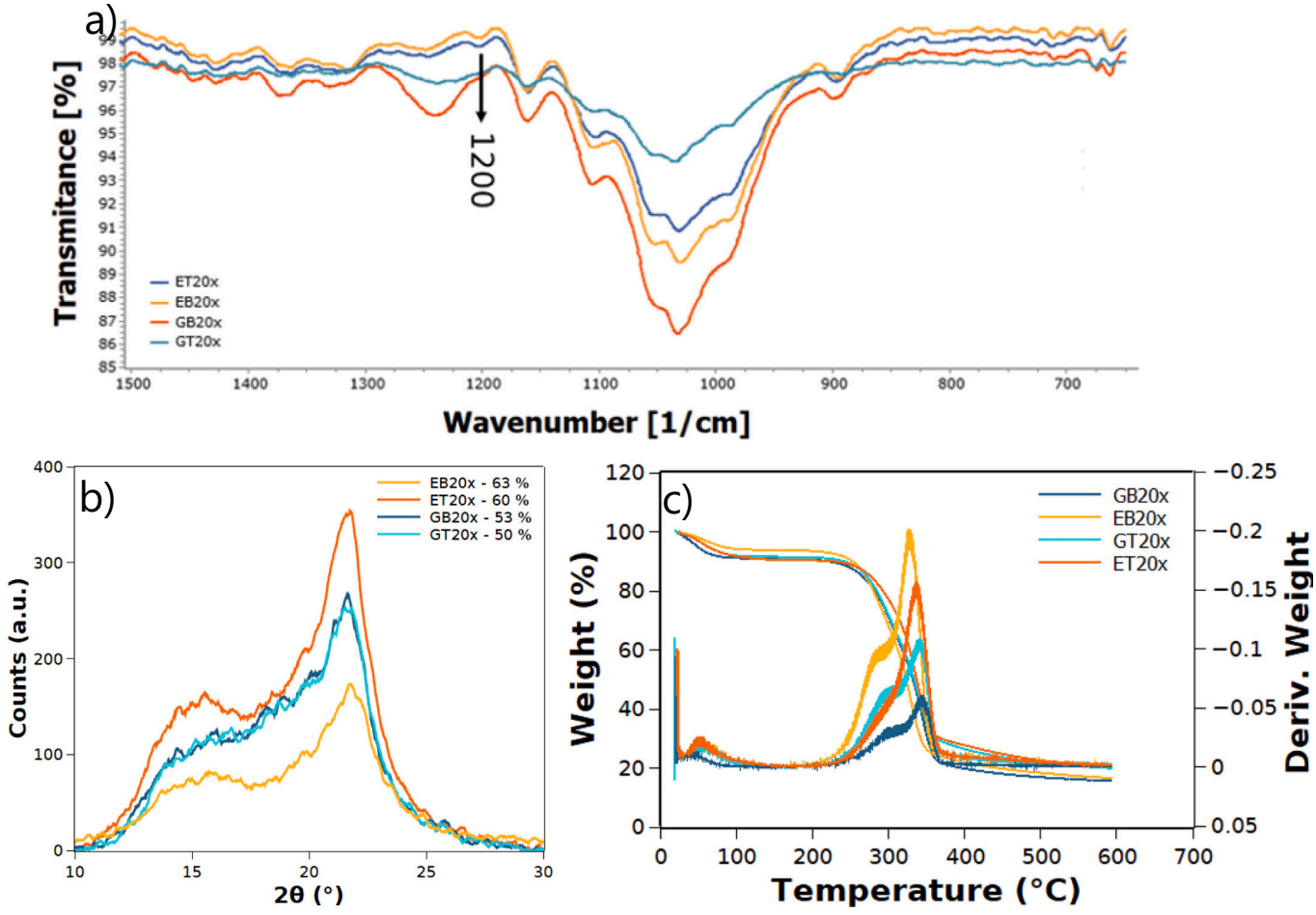

Fig. 3. a) FTIR, b) XRD and c) TGA for the samples EB20x, ET20x, GB20x and GT20x.

lower CrI [44,56].

On the other hand, in the extrusion process, the observed effect on CrI is not as pronounced. It is possible that the extrusion method, with its specific set of mechanical forces and conditions, does not induce significant disruption or rearrangement of the cellulose structure in the same manner as grinding. Further investigations are required to fully understand the underlying mechanisms and determine why the extrusion process exhibits a less pronounced impact on CrI compared to grinding.

Since TEMPO helps in facilitate the defibrillation, it is possible that an increase in viscosity occurs for the solution, as previously exposed by our group [44,56], this effect is repeated in this work. In which a decrease in crystallinity is seen with TEMPO. It is important to remind that the final sample is a film in a solvent-cast formulation, so the viscosity also plays a huge contribution to the packing and ordering.

3.6. Thermogravimetric analysis for the NFC

Fig. 3c shows the thermogravimetric analysis (TGA) for the films EB20x, ET20x, GB20x and GT20x. TGA represent the residual mass, as a function of temperature, while the DTG curves correspond to the first derivative of the TGA curves and show the variation of mass in relation to time, recorded as a function of temperature. The thermal profile observed for the cellulose showed thermal degradation between 206 and 410 °C with a DTG peak at 330 °C, with different mass residue remaining after 600 °C for samples with TEMPO and samples just with bleaching. A thermal degradation stage is detected with a shoulder peak at a lower temperature for samples defibrillated in both the extruder and the grinder. These peaks were previously reported [43]. Alves et al. (2019) reported three stages of degradation and the curve observed for them were very similar observed here. The first stage, between 24 °C and 100 °C, with a mass loss between 5 and 10 %, due to water evaporation or the loss of other volatile components. The second stage is the shoulder peak in 300 °C is the maximum degradation of the NFC. In the last stage, the degradation peak at 330 °C, with carbonized mass produced of almost 20 % [57]. The thermal degradation stability is lower for samples processed by extrusion compared to grinding, detected by the maximum degradation temperature by DTG. However, TEMPO pre-treatment similar values of degradation temperature if compared extrusion to grinding. Relating those both processes with TEMPO was able to isolate a higher yield of NFC and present similar values. When comparing the degradation stability between the two processes, extrusion tends to lead to lower degradation stability than grinding for several reasons related to chemical analysis, physical properties, and mechanical properties. Extrusion leads to lower degradation stability than grinding due to prolonged exposure to the friction generated between the material and the screw. This temperature can lead to thermal degradation of the cellulose. On the other hand, in the grinding process, there is minimal exposure to elevated temperatures, the presence of water allows greater control of non-heating. While there may be some localized heating due to the mechanical forces during grinding, it is typically not as severe as in the extrusion process. As a result, the chemical stability of the material is better preserved during grinding. Additionally, the shear and elongational forces during extrusion can cause molecular orientation and weaken the material, further reducing its mechanical properties [58,59]. Grinding, on the other hand, preserves the chemical, physical, and mechanical properties of the material to a higher extent, making it a more favorable option for materials that are sensitive to thermal degradation or require improved stability.

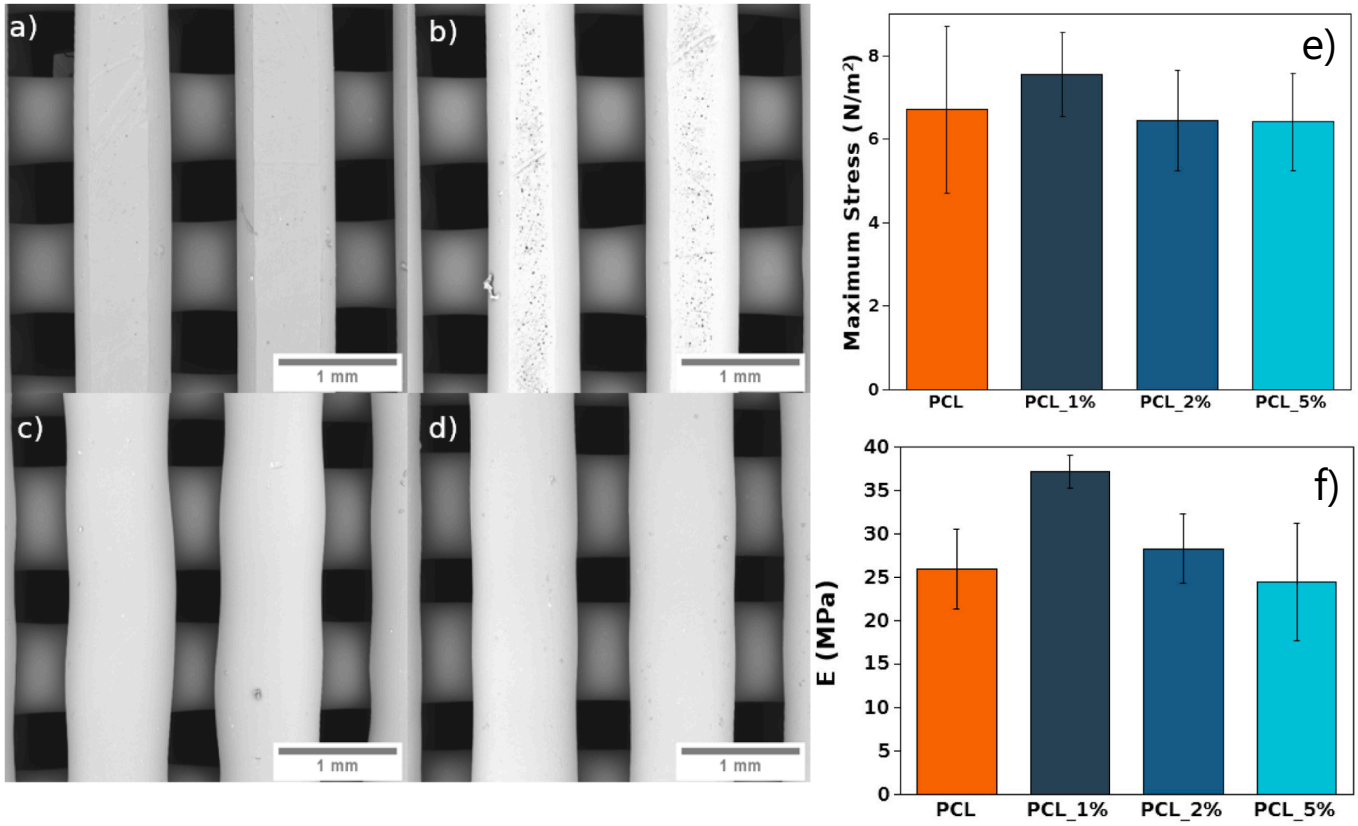

Fig. 4. The SEM images of a) PCL, b) PCL_1%, c) PCL_2%, d) PCL_5% magnification 50×. e) Compressive elastic modulus values for scaffolds samples, considering the NFC content (wt%), 1, 2 and 5 %. f) Maximum Stress for scaffolds samples, considering the NFC content (wt%), 1, 2 and 5 %. Statistically significant difference according to Tukey test ($p < 0.05$).

3.7. Morphology of the of scaffolds

The morphology of the scaffolds can be seen in Fig. 4a–d, this analysis was used to visualize the filaments and pores of scaffolds prepared with PCL and NFC. It is observed that the extruded filaments only with PCL presented a pore value of 548 μm ±13. As the cellulose concentration increases, the filament increases and consequently the pores decrease. For the samples PCL + NFC_1%, PCL + NFC_2% and PCL + NFC_5% the pore values were respectively 538 μm ± 18, 446 μm ± 17 and 437 μm ± 12. The filaments appeared to have good adhesion to adjacent filaments. It was also observed that with increasing NFC content, the extruded filaments became thicker and more wrinkled, increasing the filament width. Thus, the porosity of the scaffolds was reduced with increasing NFC concentration.

3.8. Compression resistance of scaffolds

Fig. 4a–d shows the final geometric characteristics of the scaffolds by SEM, these characteristics are determined by several factors. Patricio et al. observed differences in the geometry using just PCL and in PCL/PLA blends, these alterations were attributed to viscosity differences, caused by the higher temperature required to extrude PCL/PLA scaffolds [60]. Rashad et al. found differences in PCL scaffolds using NaOH and CNF due to a slight increase in surface area of the scaffolds compared to the PCL control [61]. In our samples, increasing the ratio of NFC changed the final geometric characteristics of the scaffolds. This was mainly attributed to viscosity due to the amount of solvent, water, in the sample, since the NFC it is used as a suspension, and it is very difficult to work as a dried NFC sample for mixing and addition with polymers due to recombination of nanofibers by intramolecular bonding.

In Table 2 can be observed the general compressive behavior of all scaffolds samples (PCL, PCL + NFC1%, PCL + NFC2% and PCL + NFC5%). Maximum stress is represented by σmax (MPa), Maximum load (MPa), compressive modulus by E (MPa) and break and all results can be observed in Table 2. Fig. 4e and f shows the compression modulus and the maximum stress values.

The sample with the highest value of compressive modulus, max load and σ max was PCL + 1%NFC with values respectively of 6825.43 MPa, 7.56 MPa, 37.14 MPa, respectively. This sample was statistically different from the PCL only sample (25.93 MPa) and from the 2 % and 5 % NFC samples. As the concentration of NFC increases to 2 % and 5 %, there was no statistical difference in relation to the scaffolds with only PCL. Increasing the cellulose concentration also increases the amount of water in the suspension for 3D printing process and the scaffold becomes weaker. Lopes et al. (2019) studied the incorporation of water in hydrogels with PEGDMA 750 and found that increasing the amount of water causes a decrease in maximum stress, as water prevents polymerization, leading to a lack of reticulated network that can better sustain the applied loads [32]. This could have occurred in this work because the suspension, as water as solvent, can lead to a lower degree of the interaction to polymerize and may lead to a weaker material.

The values found in the literature for the compressive modulus of cortical and cancellous bone varies, depending on bone density, from 90 to 230 MPa and 2 to 45 MPa, respectively [62–64]. In this work, the values obtained are close to those reported for cancellous bone and lower than those for cortical bone. Besides, many works in the literature show that the addition of NFC, even in small amounts, influenced the scaffolds mechanical response [65,66], resulting in positive results with the addition of NFC in the PCL structure.

Table 2
Mechanical tests of each scaffolds samples. Maximum stress is represented by σmax (MPa), Maximum load (MPa), compressive modulus by E (MPa) and break. * means statistically significant different by Tukey test.

Samples	Max load (N)	σmax (N/m^2)	E (MPa)	% elongation
PCL	6397 ± 1633	7 ± 2	26 ± 5	65 ± 8
PCL + NFC1%	6825 ± 1001	7.5 ± 1	37 ± 2	63 ± 4
PCL + NFC2%	5644 ± 1051	6 ± 1	28 ± 4	57 ± 6
PCL + NFC5%	5644 ± 1051	6.4 ± 2	24 ± 7	57 ± 5

3.9. In vitro cytotoxicity assay

Cell viability was performed in 24 h treatments for the PCL, PCL + 1%NFC, PCL + 2%NFC and PCL + 5 %NFC using 3T3 fibroblast cells (Fig. 5). In this work, the concentrations of 25, 5, 1 and 0.5 mg mL^{-1} were tested. The cell viability was higher than 70 % for all treatments and concentrations. This means that the prepared PCL/NFC scaffolds are biocompatible and nontoxic to the body cells.

Kuang et al. [26] used a blend with PCL and poly (ethylene oxide) to produce scaffolds and tested live/dead cell viability to detect viable cells in vitro. The authors found in vitro biocompatibility of NIH-3T3 fibroblast cell cultures with the scaffolds produced with this blend [26].

The system showed in this article can benefit from different ecosystems where the plant is inhabited and to others invasive alien plants. Even here in Ireland according to National Biodiversity Data Centre in a square area of 10.00 ha we can find 1.500 ha of Rhododendron [67]. So, this is not just a local problem from the Connemara National Park, but it is a country-wide issue. Our group has already worked with at least two other species (*Araucaria angustifolia* [16] and *Ilex paraguariensis* [18]) using this system for biomedical application. However, none with the intent of producing a 3D scaffold as it has been performed in this work.

4. Conclusion

The use of NFC for diverse applications has been increasing over time and the search for more sustainable solutions has gained greater prominence. This work arises in response to these needs. The research demonstrated that it was possible to obtain NFC from *Rhododendron ponticum* both by extrusion and by grinding process. Double screw extrusion is an interesting method because it is an equipment available in many laboratories and allows the processing and cellulose defibrillation in a higher solid content. Although extrusion may not match the defibrillation efficacy of grinding, our study demonstrated promising results in obtaining nanocellulose via the extruder, comparable to the material characteristics achieved by the grinder. It opens up the possibility of utilizing the extruder as a tool for NFC production in scenarios where cost and accessibility play crucial roles. The characteristics of the NFC produced were studied and evaluated by various characterization methods. For these Rhododendron samples, bleached and treated with TEMPO, it can be concluded that the sample with the best defibrillation results was using the grinding and oxidizing agent time after 20 passes.

Scaffolds were successfully produced according to previously outlined parameters. Through careful analysis of the morphology of the scaffolds, it was possible to conclude that the addition of NFC decreased the pore and filament sizes of the scaffolds. The manufactured scaffolds did not show toxicity to the 3T3 fibroblast cells tested in the MTT assays and show promise for biomedical applications. The scaffold produced with 1 % NFC showed the best mechanical properties as well as the highest concentrations (3 % and 5 %) did not differ statistically from pure PCL.

One of the limitations of this work is the amount of holocellulose present in the biomass. For the production of NFC, it is important that the raw wood presents an inherited high amount of cellulose. For future work, it would be interesting to add compounds with antibacterial properties. The applications of scaffolds in bone protection are numerous, and in the present work, only one type of production route was sought with a simple cytotoxicity test. A much broader study is needed to determine whether this material is appropriate for biomedical applications.

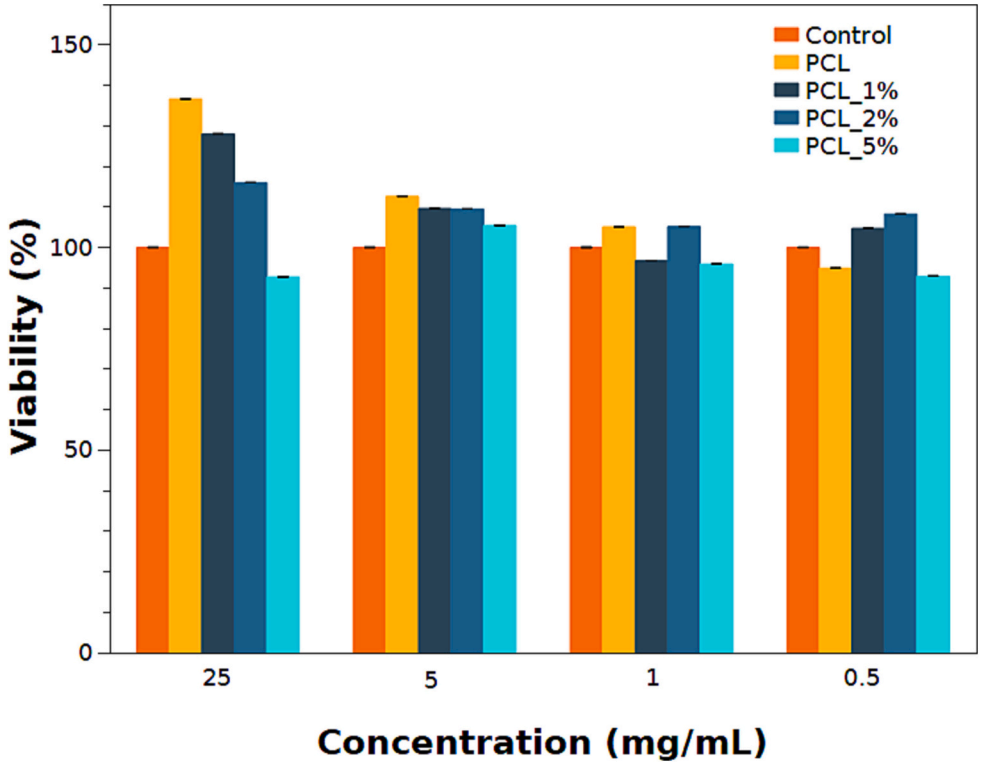

Fig. 5. In vitro cytotoxicity assay for the scaffolds with PCL, PCL + 1%NFC, PCL + 2%NFC and PCL + 5 %NFC using 3T3 fibroblast cells.

Declaration of competing interest

The authors declare that they have no known competing financial interests or personal relationships that could have appeared to influence the work reported in this paper.

Acknowledgment

The authors acknowledge the support of the Higher Education Authority and The Department of Further and Higher Education, Research, Innovation and Science.

The authors acknowledge Sean Garvey from GMIT for providing the Rhododendron samples.

References

[1] K. Noonan-Mooney, C. Gibb, How are people affecting biodiversity? Youth Guid. Biodivers. (2013) 13–21. http://www.fao.org/docrep/017/i3157e/i3157e00.htm.
[2] S. Strgulc Krajšek, E. Bahčič, U. Čoko, J. Koce, Disposal methods for selected invasive plant species used as ornamental garden plants, Manag. Biol. Invasions 11 (2020) 293–305, https://doi.org/10.3391/mbi.2020.11.2.08.
[3] Department of Agriculture Food and Marine, Rhododendron ponticum, (n.d.) 1–2.
[4] C.M. Maguire, J. Kelly, P.J. Cosgrove, Best practice management guidelines Rhododendron and Cherry Laurel (*Prunus laurocerasus*), Prep. NIEA NPWS as Part Invasive Species Irel. http://invasivespeciesireland.com/wp-content/uploads/2012/01/Rhododendron-BPM.pdf, 2008.
[5] E. Birinci, A. Tutus, M. Çiçekler, Evaluation of Rhododendron luteum and Rhododendron ponticum in pulp and paper production, Drv. Ind. 71 (2020) 365–370, https://doi.org/10.5552/drvind.2020.1943.
[6] E. Kaffashsaie, H. Yousefi, T. Nishino, T. Matsumoto, M. Mashkour, M. Madhoushi, H. Kawaguchi, Direct conversion of raw wood to TEMPO-oxidized cellulose nanofibers, Carbohydr. Polym. 262 (2021), 117938, https://doi.org/10.1016/j.carbpol.2021.117938.
[7] K. Trigui, C. De Loubens, A. Magnin, J.-L. Putaux, S. Boufi, Cellulose nanofibrils prepared by twin-screw extrusion: effect of the fiber pretreatment on the fibrillation efficiency, Carbohydr. Polym. 240 (2020), 116342, https://doi.org/10.1016/j.carbpol.2020.116342.
[8] G.G. de Lima, B. Aggio, M. Matos, T.A.M. de Lima, B.L. Pereira, A.C. Pedro, W.L. E. Magalhães, Cryoslash as an effective pre-treatment to obtain nanofibrillated cellulose using ultra-fine friction grinder with kraft pulp, Nord. Pulp Pap. Res. J. (2023), https://doi.org/10.1515/npprj-2022-0091.
[9] D. Shu, P. Xi, B. Cheng, Y. Wang, L. Yang, X. Wang, X. Yan, One-step electrospinning cellulose nanofibers with superhydrophilicity and superoleophobicity underwater for high-efficiency oil-water separation, Int. J. Biol. Macromol. 162 (2020) 1536–1545, https://doi.org/10.1016/j.ijbiomac.2020.07.175.
[10] T. Gao, G. Guan, X. Wang, T. Lou, Electrospun molecularly imprinted sodium alginate/polyethylene oxide nanofibrous membranes for selective adsorption of methylene blue, Int. J. Biol. Macromol. 207 (2022) 62–71, https://doi.org/10.1016/j.ijbiomac.2022.02.193.
[11] M. Dilamian, B. Noroozi, A combined homogenization-high intensity ultrasonication process for individualizaion of cellulose micro-nano fibers from rice straw, Cellulose. 26 (2019) 5831–5849, https://doi.org/10.1007/s10570-019-02469-y.
[12] M. Thiripura Sundari, A. Ramesh, Isolation and characterization of cellulose nanofibers from the aquatic weed water hyacinth—Eichhornia crassipes, Carbohydr. Polym. 87 (2012) 1701–1705, https://doi.org/10.1016/j.carbpol.2011.09.076.
[13] T.T.T. Ho, K. Abe, T. Zimmermann, H. Yano, Nanofibrillation of pulp fibers by twin-screw extrusion, Cellulose. 22 (2015) 421–433, https://doi.org/10.1007/s10570-014-0518-6.
[14] F. Rol, B. Vergnes, N. El Kissi, J. Bras, Nanocellulose production by twin-screw extrusion: simulation of the screw profile to increase the productivity, ACS Sustain. Chem. Eng. 8 (2020) 50–59, https://doi.org/10.1021/acssuschemeng.9b01913.
[15] F. Rol, S. Saini, V. Meyer, M. Petit-Conil, J. Bras, Production of cationic nanofibrils of cellulose by twin-screw extrusion, Ind. Crop. Prod. 137 (2019) 81–88, https://doi.org/10.1016/j.indcrop.2019.04.031.
[16] T.A. de M. de Lima, G.G. de Lima, B.S. Chee, J.G. Henn, Y.J. Cortese, M. Matos, C. V. Helm, W.L.E. Magalhães, M.J.D. Nugent, Characterization of gels and films produced from Pinhão seed coat nanocellulose as a potential use for wound healing dressings and screening of its compounds towards antitumour effects, Polymers (Basel) 14 (2022) 2776, https://doi.org/10.3390/polym14142776.
[17] M. Aliabadi, B.S. Chee, M. Matos, Y.J. Cortese, M.J.D. Nugent, T.A.M. de Lima, W. L.E. Magalhães, G.G. de Lima, M.D. Firouzabadi, Microfibrillated cellulose films containing chitosan and tannic acid for wound healing applications, J. Mater. Sci. Mater. Med. 32 (2021) 67, https://doi.org/10.1007/s10856-021-06536-4.
[18] M. Aliabadi, B.S. Chee, M. Matos, Y.J. Cortese, M.J.D. Nugent, T.A.M. de Lima, W. L.E. Magalhães, G.G. de Lima, Yerba mate extract in microfibrillated cellulose and corn starch films as a potential wound healing bandage, Polymers (Basel) 12 (2020) 2807, https://doi.org/10.3390/polym12122807.
[19] G.G. de Lima, N.B. de Miranda, T.G. Timm, M. Matos, T. Angelina Moraes de Lima, W. Luiz Esteves Magalhães, L. Benathar Ballod Tavares, F.A. Hansel, C.V. Helm, Characterisation and in vivo evaluation of Araucaria angustifolia pinhão seed coat nanosuspension as a functional food source, Food Funct. 11 (2020) 9820–9832, https://doi.org/10.1039/D0FO02256J.

[20] M. Nasir, R. Hashim, O. Sulaiman, M. Asim, Nanocellulose, in: Cellul. Nanofibre Compos, Elsevier, 2017, pp. 261–276, https://doi.org/10.1016/B978-0-08-100957-4.00011-5.
[21] D. Pradhan, A.K. Jaiswal, S. Jaiswal, Emerging technologies for the production of nanocellulose from lignocellulosic biomass, Carbohydr. Polym. 285 (2022), 119258, https://doi.org/10.1016/j.carbpol.2022.119258.
[22] N. Lavoine, I. Desloges, A. Dufresne, J. Bras, Microfibrillated cellulose – its barrier properties and applications in cellulosic materials: a review, Carbohydr. Polym. 90 (2012) 735–764, https://doi.org/10.1016/j.carbpol.2012.05.026.
[23] S.S.M. Hussain, G. Dhananjaya, A.K. Shetty, M.B. Latha, An overview on smart polymers as the backbone to hard tissue formation, ECS Trans. 107 (2022) 19163.
[24] W. Liu, H. Du, M. Zhang, K. Liu, H. Liu, H. Xie, X. Zhang, C. Si, Bacterial cellulose-based composite scaffolds for biomedical applications: a review, ACS Sustain. Chem. Eng. 8 (2020) 7536–7562, https://doi.org/10.1021/acssuschemeng.0c00125.
[25] Z. Xu, Y. Zhang, H. Dai, Y. Wang, Y. Ma, S. Tan, B. Han, 3D printed MXene (Ti2AlN)/polycaprolactone composite scaffolds for in situ maxillofacial bone defect repair, J. Ind. Eng. Chem. 114 (2022) 536–548, https://doi.org/10.1016/j.jiec.2022.07.042.
[26] T. Kuang, S. Chen, Z. Gu, Z. Shen, A. Hejna, M.R. Saeb, F. Chen, M. Zhong, T. Liu, A facile approach to fabricate load-bearing porous polymer scaffolds for bone tissue engineering, Adv. Compos. Hybrid Mater. 5 (2022) 1376–1384, https://doi.org/10.1007/s42114-022-00418-1.
[27] C. Yang, L. Zhou, X. Geng, H. Zhang, B. Wang, B. Ning, New dual-function in situ bone repair scaffolds promote osteogenesis and reduce infection, J. Biol. Eng. 16 (2022) 23, https://doi.org/10.1186/s13036-022-00302-y.
[28] J. Ge, R. Asmatulu, B. Zhu, Q. Zhang, S.-Y. Yang, Synthesis and properties of magnetic Fe3O4/PCL porous biocomposite scaffolds with different sizes and quantities of Fe3O4 particles, Bioengineering. 9 (2022) 278, https://doi.org/10.3390/bioengineering9070278.
[29] T.-T.A.O.F.T.H.E.P.A.N.D.P. INDUSTRY, TAPPI Test Methods T 222 om-88: Acid Insoluble Lignin in Wood and Pulp, 1996.
[30] S.H. Osong, S. Norgren, P. Engstrand, Processing of wood-based microfibrillated cellulose and nanofibrillated cellulose, and applications relating to papermaking: a review, Cellulose. 23 (2016) 93–123, https://doi.org/10.1007/s10570-015-0798-5.
[31] B.D. Mattos, P.H.G. de Cademartori, T.V. Lourençon, D.A. Gatto, W.L.E. Magalhães, Biodeterioration of wood from two fast-growing eucalypts exposed to field test, Int. Biodeterior. Biodegradation 93 (2014) 210–215, https://doi.org/10.1016/j.ibiod.2014.04.027.
[32] J. Lopes, R. Fonseca, T. Viana, C. Fernandes, P. Morouço, C. Moura, S. Biscaia, Characterization of biocompatible poly(ethylene glycol)-dimethacrylate hydrogels for tissue engineering, Appl. Mech. Mater. 890 (2019) 290–300, https://doi.org/10.4028/www.scientific.net/AMM.890.290.
[33] ASTM STP 1173-94, Biomaterials' Mechanical Properties, ASTM International, 1994.
[34] G. Albornoz-Palma, D. Ching, O. Valerio, R.T. Mendonça, M. Pereira, Effect of lignin and hemicellulose on the properties of lignocellulose nanofibril suspensions, Cellulose. 27 (2020) 10631–10647, https://doi.org/10.1007/s10570-020-03304-5.
[35] A. Balea, E. Fuente, Q. Tarrés, M.À. Pèlach, P. Mutjé, M. Delgado-Aguilar, A. Blanco, C. Negro, Influence of pretreatment and mechanical nanofibrillation energy on properties of nanofibers from Aspen cellulose, Cellulose. 28 (2021) 9187–9206, https://doi.org/10.1007/s10570-021-04109-w.
[36] X. Cao, B. Ding, J. Yu, S.S. Al-Deyab, Cellulose nanowhiskers extracted from TEMPO-oxidized jute fibers, Carbohydr. Polym. 90 (2012) 1075–1080, https://doi.org/10.1016/j.carbpol.2012.06.046.
[37] R. Motta Neves, K. Silveira Lopes, M.G.V. Zimmermann, M. Poletto, A.J. Zattera, Cellulose nanowhiskers extracted from tempo-oxidized curaua fibers, J. Nat. Fibers 17 (2020) 1355–1365, https://doi.org/10.1080/15440478.2019.1568346.
[38] A. Cobut, H. Sehaqui, L.A. Berglund, Cellulose nanocomposites by melt compounding of TEMPO-treated wood fibers in thermoplastic starch matrix, BioResources. 9 (2014), https://doi.org/10.15376/biores.9.2.3276-3289.
[39] I. Besbes, S. Alila, S. Boufi, Nanofibrillated cellulose from TEMPO-oxidized eucalyptus fibres: effect of the carboxyl content, Carbohydr. Polym. 84 (2011) 975–983, https://doi.org/10.1016/j.carbpol.2010.12.052.
[40] A. Isogai, T. Saito, H. Fukuzumi, TEMPO-oxidized cellulose nanofibers, Nanoscale. 3 (2011) 71–85, https://doi.org/10.1039/C0NR00583E.
[41] G.G. de Lima, E.L. de S Júnior, B.B. Aggio, B.S. Shee, E.M. de M Filho, F.A. de S Segundo, M.B. Fournet, D.M. Devine, W.L.E. Magalhães, M.J.C. de Sá, Nanocellulose for peripheral nerve regeneration in rabbits using citric acid as crosslinker with chitosan and freeze/thawed PVA, Biomed. Mater. 16 (2021), 055011, https://doi.org/10.1088/1748-605X/ac199b.
[42] F.C. Claro, C. Jordão, B.M. de Viveiros, L.J.E. Isaka, J.A. Villanova Junior, W.L. E. Magalhães, Low cost membrane of wood nanocellulose obtained by mechanical defibrillation for potential applications as wound dressing, Cellulose. 27 (2020) 10765–10779, https://doi.org/10.1007/s10570-020-03129-2.
[43] G.G. de Lima, B.D. Ferreira, M. Matos, B.L. Pereira, M.J.D. Nugent, F.A. Hansel, W. L.E. Magalhães, Effect of cellulose size-concentration on the structure of polyvinyl alcohol hydrogels, Carbohydr. Polym. 245 (2020), 116612, https://doi.org/10.1016/j.carbpol.2020.116612.
[44] L.C. Malucelli, M. Matos, C. Jordão, L.G. Lacerda, M.A.S. Carvalho Filho, W.L. E. Magalhães, Grinding severity influences the viscosity of cellulose nanofiber (CNF) suspensions and mechanical properties of nanopaper, Cellulose. 25 (2018) 6581–6589, https://doi.org/10.1007/s10570-018-2031-9.
[45] L. Solhi, V. Guccini, K. Heise, I. Solala, E. Niinivaara, W. Xu, K. Mihhels, M. Kröger, Z. Meng, J. Wohlert, H. Tao, E.D. Cranston, E. Kontturi, Understanding nanocellulose–water interactions: turning a detriment into an asset, Chem. Rev. 123 (2023) 1925–2015, https://doi.org/10.1021/acs.chemrev.2c00611.
[46] S. Fujisawa, E. Togawa, K. Kuroda, Nanocellulose-stabilized Pickering emulsions and their applications, Sci. Technol. Adv. Mater. 18 (2017) 959–971, https://doi.org/10.1080/14686996.2017.1401423.
[47] P. Yin, X. Dong, W. Zhou, D. Zha, J. Xu, B. Guo, P. Li, A novel method to produce sustainable biocomposites based on thermoplastic corn-starch reinforced by polyvinyl alcohol fibers, RSC Adv. 10 (2020) 23632–23643, https://doi.org/10.1039/D0RA04523C.
[48] P. Ek, B.-J. Gu, S.R. Saunders, K. Huber, G.M. Ganjyal, Exploration of physicochemical properties and molecular interactions between cellulose and high-amylose cornstarch during extrusion processing, Curr. Res. Food Sci. 4 (2021) 588–597, https://doi.org/10.1016/j.crfs.2021.07.001.
[49] K. Chitbanyong, S. Pitiphatharaworachot, S. Pisutpiched, S. Khantayanuwong, B. Puangsin, Characterization of bamboo nanocellulose prepared by TEMPO-mediated oxidation, BioResources. 13 (2018), https://doi.org/10.15376/biores.13.2.4440-4454.
[50] T. Thi Thanh Hop, D. Thi Mai, T. Duc Cong, T. Thi Y. Nhi, V. Duc Loi, N. Thi Mai Huong, N. Trinh Tung, A comprehensive study on preparation of nanocellulose from bleached wood pulps by TEMPO-mediated oxidation, Results Chem. 4 (2022), 100540, https://doi.org/10.1016/j.rechem.2022.100540.
[51] F. Fahma, S. Iwamoto, N. Hori, T. Iwata, A. Takemura, Isolation, preparation, and characterization of nanofibers from oil palm empty-fruit-bunch (OPEFB), Cellulose. 17 (2010) 977–985, https://doi.org/10.1007/s10570-010-9436-4.
[52] D. Trache, M.H. Hussin, C.T. Hui Chuin, S. Sabar, M.R.N. Fazita, O.F.A. Taiwo, T. M. Hassan, M.K.M. Haafiz, Microcrystalline cellulose: isolation, characterization and bio-composites application—a review, Int. J. Biol. Macromol. 93 (2016) 789–804, https://doi.org/10.1016/j.ijbiomac.2016.09.056.
[53] L. Segal, J.J. Creely, A.E. Martin, C.M. Conrad, An empirical method for estimating the degree of crystallinity of native cellulose using the X-ray diffractometer, Text. Res. J. 29 (1959) 786–794, https://doi.org/10.1177/004051755902901003.
[54] J.-F. Sassi, H. Chanzy, Ultrastructural aspects of the acetylation of cellulose, Cellulose. 2 (1995) 111–127, https://doi.org/10.1007/BF00816384.
[55] H.L. Teo, R.A. Wahab, Towards an eco-friendly deconstruction of agro-industrial biomass and preparation of renewable cellulose nanomaterials: a review, Int. J. Biol. Macromol. 161 (2020) 1414–1430, https://doi.org/10.1016/j.ijbiomac.2020.08.076.
[56] L.C. Malucelli, M. Matos, C. Jordão, D. Lomonaco, L.G. Lacerda, M.A.S. Carvalho Filho, W.L.E. Magalhães, Influence of cellulose chemical pretreatment on energy consumption and viscosity of produced cellulose nanofibers (CNF) and mechanical properties of nanopaper, Cellulose. 26 (2019) 1667–1681, https://doi.org/10.1007/s10570-018-2161-0.
[57] J.A. Andrade Alves, M.D. Lisboa dos Santos, C.C. Morais, J.L. Ramirez Ascheri, R. Signini, D.M. dos Santos, S.M. Cavalcante Bastos, D.P. Ramirez Ascheri, Sorghum straw: pulping and bleaching process optimization and synthesis of cellulose acetate, Int. J. Biol. Macromol. 135 (2019) 877–886, https://doi.org/10.1016/j.ijbiomac.2019.05.014.
[58] K. Müller, S. Fürtauer, M. Schmid, C. Zollfrank, Cellulose blends from gel extrusion and compounding with polylactic acid, J. Appl. Polym. Sci. 139 (2022), https://doi.org/10.1002/app.52794.
[59] M. Le Baillif, K. Oksman, The effect of processing on fiber dispersion, fiber length, and thermal degradation of bleached sulfite cellulose fiber polypropylene composites, J. Thermoplast. Compos. Mater. 22 (2009) 115–133, https://doi.org/10.1177/0892705708091608.
[60] T. Patrício, M. Domingos, A. Gloria, P. Bártolo, Characterisation of PCL and PCL/PLA scaffolds for tissue engineering, Procedia CIRP 5 (2013) 110–114, https://doi.org/10.1016/j.procir.2013.01.022.
[61] A. Rashad, S. Mohamed-Ahmed, M. Ojansivu, K. Berstad, M.A. Yassin, T. Kivijärvi, E.B. Heggset, K. Syverud, K. Mustafa, Coating 3D printed polycaprolactone scaffolds with nanocellulose promotes growth and differentiation of mesenchymal stem cells, Biomacromolecules. 19 (2018) 4307–4319, https://doi.org/10.1021/acs.biomac.8b01194.
[62] J.L. de Ulloa, J.E. González, A.M. Beltrán, E.P. Avés, J. Rodríguez-Guerra, Y. Torres, Biomechanical behavior of customized scaffolds: a three-dimensional finite element analysis, Mater. Des. 223 (2022), 111173, https://doi.org/10.1016/j.matdes.2022.111173.
[63] G. Hannink, J.J.C. Arts, Bioresorbability, porosity and mechanical strength of bone substitutes: what is optimal for bone regeneration? Injury. 42 (2011) S22–S25, https://doi.org/10.1016/j.injury.2011.06.008.
[64] P. Morouço, S. Biscaia, T. Viana, M. Franco, C. Malça, A. Mateus, C. Moura, F. C. Ferreira, G. Mitchell, N.M. Alves, Fabrication of poly(ε-caprolactone) scaffolds reinforced with cellulose nanofibers, with and without the addition of hydroxyapatite nanoparticles, Biomed. Res. Int. 2016 (2016) 1–10, https://doi.org/10.1155/2016/1596157.
[65] B. Nasri-Nasrabadi, T. Behzad, R. Bagheri, Preparation and characterization of cellulose nanofiber reinforced thermoplastic starch composites, Fibers Polym. 15 (2014) 347–354, https://doi.org/10.1007/s12221-014-0347-0.
[66] S.-H. Lee, Y. Teramoto, T. Endo, Cellulose nanofiber-reinforced polycaprolactone/polypropylene hybrid nanocomposite, Compos. Part A Appl. Sci. Manuf. 42 (2011) 151–156, https://doi.org/10.1016/j.compositesa.2010.10.014.
[67] The National Biodiversity Data Centre. Https://Biodiversityireland.Ie/ (n.d.).